Chapter 9
Fossil Microbodies Are Melanosomes: Evaluating and Rejecting the "Fossilized Decay-Associated Microbes" Hypothesis

ARINDAM ROY,[1] CHRISTOPHER S. ROGERS,[2] THOMAS CLEMENTS,[3]
MICHAEL PITTMAN,[1] OLIVIER HABIMANA,[4] PETER MARTIN,[5] AND JAKOB VINTHER[6]

ABSTRACT

Melanosomes are membrane-bound organelles of varying geometry, commonly found within a range of vertebrate tissues, that contain the pigment melanin. Melanosomes have been identified in the fossil record in many exceptionally preserved fossils allowing reconstructions of the coloration of many extinct animals. However, these microstructures have also been interpreted as "microbial cells" or melanin-producing bacteria based on their geometric similarities to melanosomes. Here we test these two conflicting hypotheses experimentally. Our results demonstrate multiple lines of evidence that these fossil microbodies are indeed melanosomes: the geometry of decay-associated microbes differs significantly from fossil microbodies; fossil microbodies are very strongly localized to in vivo melanized tissues and are absent in tissues typically unmelanized in vivo, in all fossils examined regardless of lithology or age.

On the basis of these results, as well as a thorough review of existing literature on melaninlike pigments, we are able to rule out a bacterial origin for fossil microbodies associated with exceptional vertebrate fossils and demonstrate that fossil microbodies are in fact preserved melanosomes.

INTRODUCTION

Integumentary coloration and patterning are instrumental to comprehending an animal's life history and evolution (Burley et al., 1982; Butcher and Rohwer, 1989). Coloration is commonly utilized by animals for aposematic signals, crypsis, sociosexual selection and optimizing physiological functions (Cuthill et al., 2017). Pigmentary systems (including melanins, carotenoids and porphyrins) produce coloration through selective absorbance and reflectance of wavelengths of light (Hill and McGraw, 2006a; 2006b). Additionally, structural integumentary coloration is produced by scattering of different wavelengths of light due to nanoscale variations in refractive indices of the tissue constituents making up the integumen-

[1] Vertebrate Palaeontology Laboratory, Division of Earth and Planetary Science, the University of Hong Kong, Hong Kong.
[2] School of Biological, Earth and Environmental Sciences and Environmental Research Institute, University College Cork, Cork, Ireland.
[3] School of Geography, Earth and Environmental Sciences, University of Birmingham, Edgbaston, Birmingham, U.K.
[4] School of Biological Sciences, the University of Hong Kong, Hong Kong.
[5] Interface Analysis Centre, H.H. Wills Physics Laboratory, School of Physics, University of Bristol, Bristol, U.K.
[6] School of Earth Sciences, University of Bristol, Bristol, U.K.

tary structures (Prum, 1999). Melanin pigments are widespread among vertebrates and have garnered much interest within the paleontological community in the last decade (Vinther et al., 2008, 2010, 2015, 2020; Li et al., 2010, 2012; Clements et al., 2016; McNamara et al., 2016; Roy et al., 2020) especially because the identification of fossilized pigments has allowed the color of extinct organisms to be interpreted, which has provoked significant scientific and cultural interest (Vinther, 2015, 2020; Roy et al., 2020). What makes melanin especially important to fossil color reconstruction is its intrinsic synthesis as a metabolic product (rather than the result of dietary uptake, e.g., carotenoids), and its potential for preservation in various taxa across deep time (Vinther et al., 2008; Glass et al., 2012).

Melanin is most commonly found within vertebrates encased within lysosome-derived, membrane-bound and subcellular vesicles called melanosomes (Raposo et al., 2001). Melanosomes have been described in fossil fish (Lindgren et al., 2012; Tanaka et al., 2014; Clements et al., 2016; Gabbott et al., 2016), amphibians (McNamara et al., 2016, Rossi et al. 2019), marine reptiles (Lindgren et al., 2014), birds (Clarke et al., 2010; Pan et al., 2016; Gren et al., 2017; Zheng et al., 2017), nonavialan dinosaurs (Li et al., 2010, 2012; Zhang et al., 2010; Xu et al., 2015; Vinther et al., 2016; Hu et al., 2018) and mammals (Manning et al., 2019; Rossi et al., 2019).

Animal melanins create a spectrum of colors within a tissue by varying the ratio of dark-brown/black, produced by eumelanin, and rufous to buff, produced by pheomelanin (Vinther et al., 2008). Observations of extant mammalian and avian melanosomes show a geometrical continuum from spherical to "elongate-oblong" shapes. The elongate-oblong integumentary melanosomes that contain high relative proportions of eumelanin and have been termed "eumelanosomes," whereas spherical melanosomes are typically dominated by pheomelanin and are called "pheomelanosomes" (Hill and McGraw, 2006b). It is important to appreciate, though, that natural melanosomes will vary in composition and the eumelanosome/phaeomelanosome dichotomy is only crudely instructive in describing this observed variation.

The reconstruction of color patterns in ancient animals is a burgeoning field of paleontological research and is intricately linked with the geometry of melanin-bearing "melanosome-like microbodies" (Moyer et al., 2014; Lindgren et al., 2015; Schweitzer et al., 2015) preserved in fossils. Investigations into the distribution of melanosomes in fossils led to the identification of countershading in extinct animals allowing ecological and behavioral implications to be inferred (Vinther et al., 2016; Brown et al., 2017; Smithwick et al., 2017). However, the identity of such "microbodies" has been repeatedly called into question, with a counter view (Wuttke, 1983; Toporski et al., 2002; Moyer et al., 2014; Lindgren et al., 2015; Schweitzer et al., 2015) that interprets them as fossilized microbial cells, which they were traditionally identified as, prior to the work of Vinther et al. (2008). This traditional view has been challenged in several studies evaluating the evidence for these microbodies being melanosomes, based on four important characteristics: (1) geometric and spatial consistency with extant melanosomes (Vinther et al., 2008; Li et al., 2010; Zhang et al., 2010; Li et al., 2012); (2) concentration of microbodies in fossilized vertebrate tissues that originally contained melanosomes, i.e., feathers, eyes, and visceral organs (Vinther et al., 2008; Zhang et al., 2010; Gabbott et al., 2016); (3) preserved color patterns (Vinther et al., 2008); and (4) presence of chemical signatures of melanin-derived compounds in the microbodies (Glass et al., 2012 , 2013; Colleary et al., 2015).

Despite this body of direct and indirect evidence, a consensus regarding the identity of fossil microbodies has yet to be reached. Four main counterarguments have been posited in favor of the microbial identity of fossil micro-

TABLE 1

Melanosomes measured from feathers of modern birds

No..	Species sampled	Feather color	Sample size	Melanosome shape
1	*Tragopan* sp.	Black	162	Elongate rod
2	Sunbittern (*Eurypyga helias*)	Dark brown	100	Spherical/oblate
3	Turaco (species unknown)	Iridescent	144	Elongate rod
4	Palawan peacock-pheasant (*Polyplectron napoleonis*)	Iridescent	150	Elongate rod
5	Chicken (*Gallus gallus*)	Iridescent tructural	50	Oblong
6	Black-throated trogon (*Trogon rufus*)	Iridescent structural	50	Elongate rod
7	Bar-tailed trogon (*Apaloderma vittatum*)	Iridescent structural	60	Elongate rod
8	Eurasian kingfisher (*Alcedo atthis*)	Noniridescent structural	65	Oblong
9	Black-capped kingfisher (*Halcyon pileata*)	Noniridescent structural	70	Oblong
10	Blue cuckooshrike (*Coracina azurea*)	Noniridescent structural	80	Elongate rod/ oblong
11	Ivory-breasted pitta (*Pitta maxima*)	Noniridescent structural	70	Oblong
12	Rock dove (*Columba livia*)	Gray	150	Elongate rod
13	Victoria crowned pigeon (*Goura victoria*)	Gray	131	Spherical/oblong

bodies (Moyer et al., 2014; Lindgren et al., 2015; Schweitzer et al., 2015): (1) frameworks seen in fossil microbodies are formed because microbes align themselves in biofilms (Toporski et al., 2002; Moyer et al., 2014); (2) decay-related microbes readily colonize dead bodies and so would naturally be preserved and more readily visible than melanosomes, which would instead be encapsulated by fossilized keratin out of view (Toporski et al., 2002; Moyer et al., 2014; Schweitzer et al., 2015); (3) microbes are ubiquitous, fossilize easily, and are indistinguishable geometrically from melanosomes (Moyer et al., 2014; Schweitzer et al., 2015); and (4) certain microbes (bacteria and fungi) produce melanin pigments that may lead to erroneous chemical identification rather than the melanin in the tissues of the organism itself (Lindgren et al., 2015; Schweitzer et al., 2015). Herein, we test the validity of these arguments, by designing experiments to test the following hypotheses:

(1) Melanosomes and microbial cells are geometrically indistinguishable

(2) Microbes localize and align themselves in orientations akin to extant melanosomes

(3) Microbes fossilize easily and are thus ubiquitous throughout fossils

(4) Microbes are sources of melanin and there is a likelihood of extraneous preservation in fossils.

TABLE 2

Microbody samples measured from isolated fossil feather specimens

No.	Material	Accession code	Sample size	Microbody shape	Source
1	feather	LEUIG 115562	40	Elongate rod	Crato formation, Brazil
2	feather	SMF-ME 3850	60	Elongate rod	Grube Messel, Germany
3	feather	MORS-1003	32	Elongate rod	Island of Mors, Fur Formation, Denmark
4	feather	SMF-ME 3830 (microbody type 1)	54	Elongate rod/ oblong	Grube Messel, Germany
5	feather	SMF-ME 3830 (microbody type 2)	31	Oblong/spherical	Grube Messel, Germany
6	feather	SMF-ME 3800B	40	Elongate rod/ oblong	Grube Messel, Germany
7	feather	SMF-ME 3721	30	Elongate rod	Grube Messel, Germany
8	feather	SMF-ME 3719A	40	Elongate rod	Grube Messel, Germany
9	feather	SMF-ME 3815	40	Elongate rod	Grube Messel, Germany

TABLE 3

Fossilised feather specimens associated with skeletal material, used for sampling and measurement of microbodies

No.	Specimen	Accession code	Sample size	Microbody shape	Taxon	Source
1	Danekræ 200	MGUH 28.929	40	Elongate rod	Aves	Fur, Denmark
2	*Eocypselus vincenti*	MHUG 26729	40	Elongate rod/ oblong	Aves	Fur, Denmark
3	*Eocoracias* sp.	Un-accessioned	35	Elongate rod/ oblong	Aves	Grube Messel, Germany
4	Unknown feather with tail	FUM-N 2275	34	Elongate rod	Aves	Fur, Denmark
5	*Hassiavis laticauda*	HLMD-ME 9047a	50	Elongate rod	Aves	Grube Messel, Germany
6	*Messelirrisor halcyrostris*	SMF-ME 10987b	40	Elongate rod	Aves	Grube Messel, Germany
7	Unknown (with head crest)	HLMD-ME 15634a	50	Elongate rod/ oblong	Aves	Grube Messel, Germany
8	*Anchiornis huxleyi* (microbody type 1)	BMNHC PH828	40	Spherical/ oblate	Avialae	Liaoning, China
9	*Anchiornis huxleyi* (microbody type 2)	BMNHC PH828	40	Elongate rod/ oblong	Avialae	Liaoning, China
10	*Microraptor gui*	BMNHC PH881	50	Elongate rod/ oblong	Dromaeosauridae	Liaoning, China

TABLE 4

Fossil anuran specimens used for sampling and measurement of microbodies

No.	Specimen	Accession code	Sample size	Microbody shape	Taxon	Material	Formation
1	*Pelobates* sp.	PW 2005-5034LS_ GDKE	60	Spherical/oblate	Anuran tadpole	Skin	Enspel, Germany
2	Pipidae	MU 41-13	50	Spherical/oblate	Anura	Skin	Mush valley, Ethiopia
3	*Paleobatrachus* sp.	SMF-ME 11390a	70	Spherical/oblate	Anura	Skin	Messel, Germany

MATERIALS AND METHODS

Sampling of Melanosome Geometry through Scanning Electron Microscopy

Modern melanosomes were extracted from the feathers of 13 extant birds (table 1) and the skin and liver of *Xenopus* sp. Melanin extracts and tissue samples from decay experiments were air dried, affixed to aluminium stubs with double-sided carbon tape, and sputter-coated with gold. Fossil microbody samples were measured from SEM images of exceptionally preserved specimens (tables 2–4). Modern melanosomes and fossil microbodies were imaged at an accelerating voltage of 5–15 keV using a Hitachi 3500N SEM. Melanosomes and microbodies were measured using Image J v.1.52 (Schneider et al., 2012).

Decay Experiments to Investigate the Geometry of Microbial Cells

Actuopalaeontological laboratory experiments (Valentine, 1989; Kowalewski, 1999; Briggs and Crowther, 2008; Sansom, 2014; Zuschin and Ebner, 2015) modeling decay under submerged, freshwater lacustrine, marine, and estuarine conditions, were carried out on a range of specimens: (1) isolated feathers (table 5), (2) bird carcasses (table 6) and (3) clawed frog (*Xenopus* sp.) tadpole carcasses (table 7). Chicken (*Gallus gallus*) and golden pheasant (*Chrysolophus pictus*) feathers were chosen for this experiment due to their availability and range of colors as well as their prior experimental use to facilitate comparisons with these studies (Ichida et al., 2001; Moyer et al., 2014; Schweitzer et al., 2015). Recently deceased bird carcasses were provided by the Royal Society for the Prevention of Cruelty to Animals (RSPCA).

Isolated feathers and bird carcasses were placed in individually sealed vessels of two sizes, 250 ml and 1 L, filled with either pond water or mineral water with estuarine sediment. Within 250 ml glass jars, isolated feathers were submerged in: (1) 180 ml of pond water, sparing amounts of pond sediment (<5 g), and small amounts of algal material, and (2) 180 ml of mineral water with fresh sediment (30 g) collected from the Severn estuary mudflats. The isolated feather decay experiments were conducted over two- and four-week intervals. Whole carcasses of two British Dipper (*Cinclus cinclus gularis*) and Eurasian Kingfisher (*Alcedo atthis*) were placed in separate 1 L containers. One specimen of *C. gularis* was submerged in 750 ml of pond water (<5 g sediment/container). The other *C. gularis* and *A. atthis* carcasses were submerged in 120 g (wet weight) of estuarine sediment and 750 ml of mineral water. All three carcasses were secured underwater using a plastic mesh. One feather was sampled from each whole bird carcass at several locations (head and neck, back, breast, wings, flank, abdomen and tail) at one- and two-week intervals. Additionally, *Xenopus* sp. tadpoles, euthanized in accordance with Schedule 1 of the United Kingdom Animals (Scientific Procedures) Act (1986), were

TABLE 5

Treatments, sample sizes and bacterial morphotypes observed in isolated feather decay experiments
(* measured from Ichida et al., 2001: fig. 6)

No.	Isolated feathers	Decay time	Treatments	Sample size	Bacterial morphotypes
1	Keratin digesting bacteria	4 weeks	*	35	baciliform, coccoid, coccobaciliform
2	Black chicken feather	2 weeks	Estuarine sediment + mineral water	42	baciliform, coccoid
3	Black chicken feather	2 weeks	Pond water	100	baciliform, coccoid, flagellated vibrio, fusiform
4	White chicken feather	2 weeks	Pond water	45	baciliform, coccoid
5	Variegated golden pheasant feather	2 weeks	Pond water	80	baciliform, coccoid, vibrio, actinomycetes
6	Black chicken feather	4 weeks	Pond water	68	baciliform, coccoid, actinomycetes
7	White chicken feather	4 weeks	Pond water	28	baciliform, coccoid
8	Variegated golden pheasant feather	4 weeks	Pond water	49	baciliform, coccoid, coccobaciliform vibrio, actinomycetes
9	Black chicken feather	4 weeks	Cyanobacterial tank	111	baciliform, coccoid
10	White chicken feather	4 weeks	Cyanobacterial tank	45	baciliform, coccoid

submerged in small 43 ml sealed containers filled with 32 ml of pond water. Three tadpoles (~3 cm long) were sampled after 1, 2, and 5 days of decay. Each individual sealed container was maintained at 22.5° C ± 0.1° C within a temperature-controlled incubator. Isolated feathers were also placed at the bottom of a tank (35 cm × 24 cm × 22 cm) containing artificial sea water, cyanobacterial blooms as well as a variety of marine microflora and fauna that had grown and stabilized over a period of more than six months. Feathers were harvested from the tanks after four weeks. The temperature for the cyanobacterial tank experiment was maintained between 20°–26° C.

All the tissue samples were fixed using 10% neutral buffered formalin (for 30 minutes) and dehydrated using standard histological techniques (Suvarna et al., 2019). Samples were critical point dried (using CO_2 gas), mounted on aluminum stubs using double-sided carbon tape and sputter-coated with gold. The stubs were imaged using a Hitachi S-3500N SEM.

Measurements and Statistical Data Analysis

Length, diameter, and aspect ratio (length ÷ diameter) of melanosomes (n = 1521), microbodies from exceptionally preserved fossils (n = 927) and microbial cells from decay experiments (n = 2117) were measured. These measurements were pooled into three categories based on their source. The raw data are available at Dryad (https://doi.org/10.5061/dryad.xgxd254dj). Statistical tests were employed to better understand the extent of geometrical overlap between melanosomes, fossil microbodies, and decay-associated microbes.

The datasets were first standardized and the residuals were examined for normality using the Kolmogorov-Smirnov (KSL) and Shapiro-Wilk (S-W) goodness-of-fit tests (Yap and Sim, 2011) using JMP, 14.0 (SAS Institute Inc., 1989–2019). Secondly, since the residuals for all three categories have significant departures from normality ($p < 0.001$), we opted for nonparametric analytical methods (Lehmann, 2006) of comparing

TABLE 6

Treatments, sample sizes and bacterial morphotypes observed in bird carcass associated feather decay experiments

(– indicates no microbial growth)

Bird carcass	Treatment	Feather location	Feather color	Sample size	Decay time	Bacterial morphotypes
British Dipper (*Cinclus cinclus gularis*) #1	Pond water	Head & neck	Black	58	1 week	Baciliform, coccoid, coccobaciliform
		Shoulder	Black	86	1 week	Baciliform, club-rod
		Breast	Black-tipped white	31	1 week	Baciliform, vibrio, spirochaete
		Flank	Grayish black	27	1 week	Baciliform
British Dipper (*Cinclus cinclus gularis*) #2	Estuarine sediment + mineral water	Head & neck	Black	–	1 week	–
		shoulder	Black	-	1 week	–
		Breast	Black-tipped white	43	1 week	Baciliform
		Flank	greyish black	19	1 week	Baciliform, actinomycetes
Eurasian Kingfisher (*Alcedo atthis*)	Estuarine sediment + mineral water	Head (back)	Gray	94	1 week	Baciliform, coccoid, coccobaciliform, actinomycetes
		Shoulder	Greenish blue	35	1 week	Baciliform
		Abdomen	White & ginger with black tip	–	1 week	–
		Tail	Pale blue	95	1 week	Baciliform
British Dipper #1	Pond water	Head & neck	Black	112	2 weeks	Baciliform, coccobaciliform, actinomycetes
		Shoulder	Black	61	2 weeks	Baciliform, coccobaciliform, actinomycetes
		Breast	Black-tipped white	52	2 weeks	Baciliform, coccobaciliform,
		Flank	Grayish black	115	2 weeks	Baciliform, coccoid, coccobaciliform
British Dipper #2	Estuarine sediment + mineral water	Head & neck	Black		2 weeks	Baciliform, club rod
		shoulder	black	75	2 weeks	Baciliform, coccoid, coccobaciliform
		breast	Black-tipped White	80	2 weeks	Baciliform, club rod
		Flank	Grayish black	41	2 weeks	Baciliform, coccoid, fusiform, actinomycetes

TABLE 6 *continued*

Bird carcass	Treatment	Feather location	Feather color	Sample size	Decay time	Bacterial morphotypes
Eurasian Kingfisher	Estuarine sediment + mineral water	Head (back)	Gray	–	2 weeks	–
		Shoulder	Greenish blue	106	2 weeks	Baciliform, fusiform, actinomycetes
		Abdomen	White & ginger with black tip	97	2 weeks	Baciliform, coccoid, actinomycetes
		Tail	Pale blue	42	2 weeks	Baciliform

medians, followed by multiple comparisons (Neuhäuser and Bretz, 2001; for nonpooled analyses using rarefied taxonomic groups, see appendix 1 in the online supplement at: doi.org/10.5531/sd.sp.44). Additionally, principal components analysis (PCA), which has been previously used to separate characteristic ToF-SIMS peaks in the chemical discrimination of fossilized melanin pigments (Colleary et al., 2015), has also been utilized in this study to further visualize the differences between each category's geometrical space. In parallel to pairwise comparisons and PCA, we also log-transform and reexpress the two initial independent variables into two new parameters:

$$\text{Shape} = \log(\text{length}) + \log(\text{diameter}) \quad (1)$$
$$\text{Size} = \log(\text{length}) - \log(\text{diameter}) \quad (2)$$

While shape parameter (1) serves as an estimate of the area, a size parameter (2) captures an estimate of aspect ratio, both of which can adequately characterize regular shapes. Since one of the major questions investigated by this study is the possibility of discriminating between our three sources of data, two statistical methods, discriminant analysis and logistic regression, could potentially be of interest. To accurately capture the estimates of area and aspect ratio, length and diameter were operationalized into variables, i.e., size and shape. However, none of the categories seem to show normal distribution as evidenced by low goodness-of-fit values from KSL test and Normal quantile plots. Since normality of factor distributions is an important assumption for discriminant analysis applied to categorize melanosome types (Li et al., 2010, 2012; Hu et al., 2018), it cannot be applied in this case. Hence, logistic regression, which does not assume any normality of distribution in fitting a nominal multilevel response to independent explanatory variables, was the method of choice. The sources of the data were categorized into three response levels (modern melanosomes, fossil microbodies, and decay-associated microbes) of the dependent variable "Type" (Y, Response). (1) and (2) then become the independent predictor variables (X, Factors). Nominal logistic regression of the two predictor variables (1) and (2) were performed on "Type" first individually to examine the cumulative probability plots and then multinomially to estimate the probabilities of choosing one of the three response levels as a smooth function of the independent explanatory variables.

SURVEY OF BEDDING PLANES IN EXCEPTIONALLY PRESERVED FOSSILS

The matrix of seven exceptionally preserved fossils were investigated using a Zeiss Sigma HD VP Field Emission SEM (FE-SEM) to assess the prevalence of microbodies present in the matrix (table 8). Areas of the fossil likely to be heavily melanized in life (e.g., eyes, feather barb/barbules) were marked with copper tape pointers. A 3×3 grid with nine centered points, each at a vertical

TABLE 7

Treatments, sample sizes and bacterial morphotypes observed in tadpole decay experiments

Xenopus Tadpole	Treatment	Sample size	Decay time	Bacterial morphotypes
#1	Pond water	183	1 day	Baciliform, coccoid, coccobaciliform, vibrio, streptobacilli
#2	Pond water	124	2 days	Baciliform, coccoid, coccobaciliform, streptobacilli

and horizontal distance of 100 μm apart were set up at the rear ends of the copper tape pointer in the matrix. In each specimen a total area of 8748 μm^2 of the matrix was scanned for microbodies.

RESULTS

Decay Experiments on Isolated Feathers and Carcasses

Isolated chicken (*Gallus gallus*) and golden pheasant (*Chrysolophus pictus*) feather samples decayed in pond water, yielded microbial growth after one week and two weeks of decay respectively. SEM images revealed microbial activity on the surface of barbs, barbules, and the rachis of feathers after one and two weeks of decay in brackish and freshwater conditions. The major bacterial morphotypes observed include rod-shaped, spherical, helical, commashaped, and stalked subspherical forms (table 5). One black feather that had decayed for two weeks using sediment inoculum showed randomly oriented bacterial cells with diverse geometry, ranging from bacilliform and coccoid cells to stalked spherical forms. Some of the bacilliform cells were captured in a state of division (fig. 4K).

After one and two weeks of decay, the major bacterial morphotypes observed on the isolated feathers also appear on feathers removed from the whole bird carcasses (fig. 4H–K, table 6). The *Xenopus* tadpoles showed a dense accumulation of bacterial and fungal growth on the wrinkled and partially degraded epidermis after one and two days of decay. After five days the tadpole body had completely disintegrated, so microbes could not be visualized. The morphotypes of microbes observed include rod-shaped and subspherical cells often forming chainlike or three-dimensional multicellular aggregate structures (fig. 4I, table 7).

Statistical Appraisal of the Geometrical Similarity in Melanosomes, Fossil Microbodies, and Decay-Associated Microbial Consortia

KSL and S-W goodness-of-fit tests for the residuals for all three categories show statistically significant deviation from normal distributions, necessitating the use of nonparametric tests. Thus, to avoid violating the normality assumptions for one-way analysis of variance (ANOVA), Wilcoxon/Kruskal Wallis (rank sums) was opted for, which independently demonstrated that for all three variables—length, diameter, and aspect ratio—the null hypothesis (H_0: samples originate from identical populations) was rejected in favor of the alternative hypothesis (H_A: samples originate from dissimilar populations). Multiple pairwise comparisons to further scrutinize the differences between the three categories, the Steel-Dwass method (a nonparametric alternative to the parametric Tukey-Kramer test) exhibited significant differences ($p < 0.0001$) between all possible pairs (modern melanosomes; fossil microbodies, fossil microbodies; decay-associated microbes, modern melanosomes; decay associated microbes) for all three variables. The Hodges-Lehmann statistic (an estimate of the median of the difference) indicates the extent of the differences between the pair (table 9).

The observations from the significant Steel-Dwass test ($p < 0.05$) show that when all three of the parameters are used to make pairwise com-

TABLE 8

Specimens used in survey of bedding planes for preserved microbes

No.	Specimen	Accession code	Taxon	Location
1	Isolated feather	IVPP V15388B	Avialae	Jehol Group, N.E. China
2	Isolated feather	MORS-1003	Aves	Fur Formation, Denmark
3	*Antigonia* sp.	Unaccessioned	Actinopterygii	Ølst formation, Denmark
4	*Esconicthys apopyris*	ROM56792	Dipnoi	Mazon Creek, IL
5	*Acanthodes* sp.	PF11509	Acanthodii	Mazon Creek, IL
6	*Acanthodes* sp.	ROM56807	Acanthodii	Mazon Creek, IL
7	*Bandringa rayi*	ROM56789A	Chondrichthyes	Mazon Creek, IL

TABLE 9

Steel-Dwass multiple comparison tests with the Hodges-Lehmann statistics
(* indicates significant differences)

	Pairwise comparisons		p Value	Hodges-Lehmann
Length	Modern melanosomes	Fossil microbodies	<.0001*	-0.112000
	Fossil microbodies	Decay-associated microbes	<.0001*	-0.358000
	Modern melanosomes	Decay-associated microbes	<.0001*	-0.463000
Diameter	Modern melanosomes	Fossil microbodies	<.0001*	-0.071000
	Fossil microbodies	Decay-associated microbes	<.0001*	-0.156000
	Modern melanosomes	Decay-associated microbes	<.0001*	-0.229000
Aspect ratio	Modern melanosomes	Decay-associated microbes	<.0001*	0.4592003
	Fossil microbodies	Decay-associated microbes	0.0006*	0.2450064
	Modern melanosomes	Fossil microbodies	0.0003*	0.2753790

parisons between modern melanosomes and fossil microbodies, the values of Hodges-Lehmann statistic are the least. Lower values of the Hodges-Lehmann statistic indicate that there is very little difference between the two categories. Additionally, the pairwise relative differences between the other two categories (fossil microbodies and decay-associated microbes; modern melanosomes and decay-associated microbes) elicit the largest values for Hodges-Lehmann statistic indicating that these pairs are very different from each other.

Secondly, PCA also provides further evidence of the distinction between the three categories using the same variables: length, diameter, and aspect ratio. The two-main principal components accounted for 83.84% of the total variance, with PC1 and PC2 accounting for a variance of 43.28% and 40.56% respectively. PC1 was positively correlated with long-axis description parameter, whereas PC2 was negatively correlated with short-axis description parameter (see table 10 for eigenvalues and loadings). The score plot (fig. 1), revealed the presence of two main

TABLE 10

Importance of components and component score coefficients' matrix obtained from PCA

	PC1	PC2	PC3	PC4
Standard deviation	1.3155	1.2737	0.7550	0.2778
Proportion of variance	0.4328	0.4056	0.1425	0.0193
Cumulative proportion	0.4328	0.8382	0.9807	1.0000

	PC1	PC2
Length	0.9469427	0.0569732
Diameter	0.2407538	-0.8809818
Aspect ratio	0.6956320	0.6941172
Type	0.5403630	-0.6008939

groupings, one composed of microbial cells and the other composed of fossils and melanosome microbodies. Results indicate that microbial cells are highly variable in terms of long-axis measurements, and larger in short-axis measurement parameters. Melanosomes and fossil microbodies were, unlike bacterial cells, better described as having the smaller short-axis and moderate long-axis measurements.

Finally, individual logistic fits of "Type" against shape (χ^2 = 56.070, p <0.0001) and size (χ^2 = 2607.614, p <0.0001) both show statistical significance (fig. 2). Better model fit is exhibited by size (R^2 = 0.2730) compared to shape (R^2 = 0.0059); therefore, size is more important in classification of the collected data into modern melanosomes, fossil microbodies, and decay-associated microbodies. This receives further support through the misclassification rate, which is comparatively lower for size (33.03%) than for shape (52.46%). When shape and size, taken together, were regressed against Type, the logistic fit was still statistically significant (χ^2 = 2757.983, p <0.0001), the model fit improves (R^2 = 0.2887) and the misclassification rate drops to 32.31%. Lack-of-fit test for the combined logistic regression is also statistically significant (χ^2 = 6769.544, p ≈ 1), also suggesting that the model fit is quite good. Given that there are three response levels to the dependent variable Type, a misclassification rate cutoff for statistically nonsignificant classification would be 66%. Thus, the results show that we can indeed classify the collected geometrical data based on the source, i.e., melanosomes from modern animals, microbodies from fossils and microbial cells associated with decay of tissues.

Survey of Fossil-Bearing Bedding Planes

All fossils exhibited localization of microbodies to the tissues and organs that were melanin bearing in life (fig. 3; see also figs. S3–S9 in the online supplement at: doi.org/10.5531/sd.sp.44). Organic microbodies preserved in three dimensions appear in the feather from the Fur Formation (MORS-1003), but the adjacent matrix sampled in the 3 × 3, 100 μm grid yielded no microbodies either as organic structures or impressions (see fig. S9 in appendix 2 in the online supplement at: doi.org/10.5531/sd.sp.44). The same was the case for the feather from Jehol Group (IVPP V15388B), although the microbodies here were preserved only as impressions (see fig. S8 in appendix 2 in the online supplement at: doi.org/10.5531/sd.sp.44). Microbodies in the feathers were furthermore aligned along the barb and barbule axes. The eyes of all Mazon Creek specimens examined in this study and *Antigonia* sp. (Bonde, 1997) from the Fur Formation (see figs. S4–S9 in appendix 2 in the online supplement: doi.org/10.5531/sd.sp.44) display clusters or layers of distinct oblong and oblate microbodies. Like the feathers

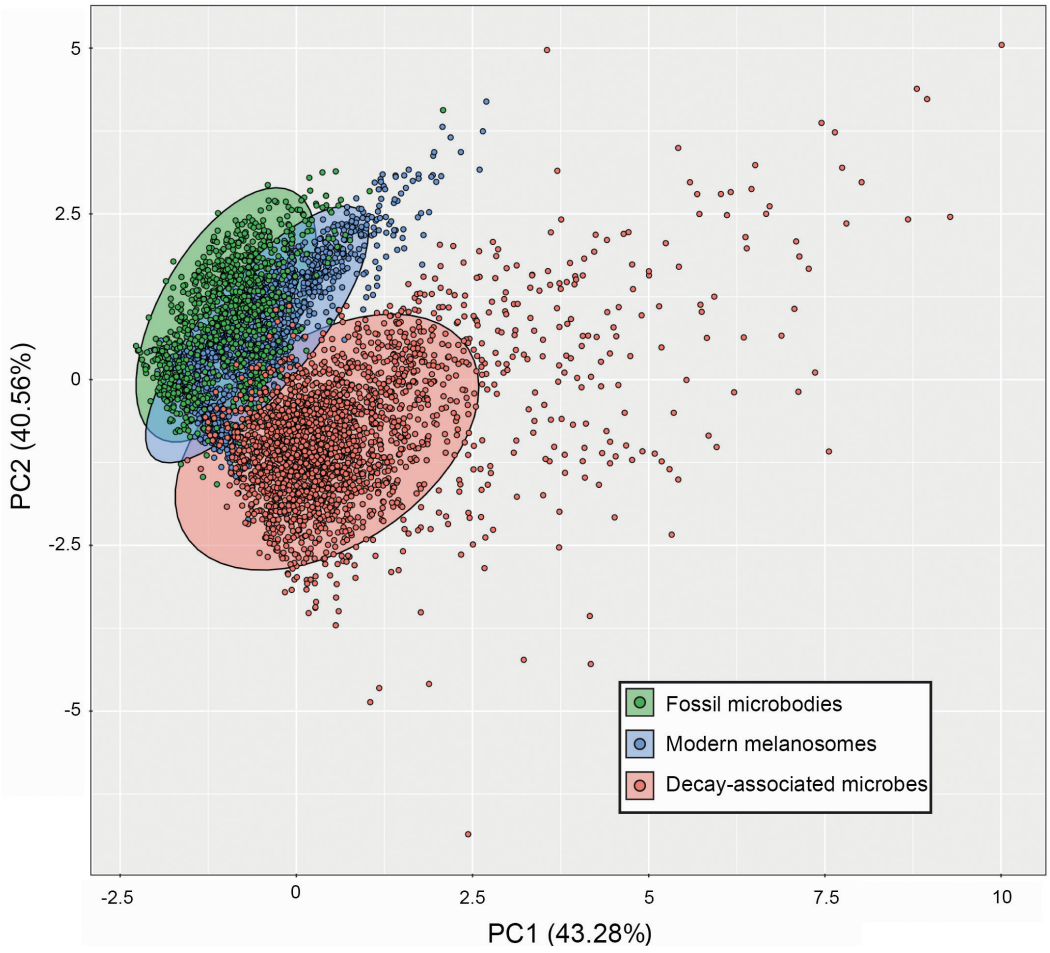

FIG. 1. PCA plot with PC1 and PC2 as axes establishes the presence of two main groupings, one composed of microbial cells and the other composed of intermingled fossils and melanosome microbodies populations; 95% confidence intervals shown by colored ellipses.

examined, the systematic survey of the adjacent matrix yielded no microbodies. Pockets of pyrite framboids appear quite frequently in the matrix but are easily distinguishable from coccoid bacterial cells by their less rounded, regular crystalline facets and framboidal habits.

DISCUSSION

Decay Experiments

The results of the decay experiments demonstrate that geometrically diverse microbes colonize isolated feathers and carcasses (fig. 4). While some microbes do overlap with melanosomes in shape, their size distribution is broader and exceeds the range of sizes observed in melanosomes (fig. 1). Bacterial cells in our experiments are not observed to concentrate or align themselves along barbs or barbule axes like melanosomes in any of our experiments, allowing the rejection of the hypothesis that microbes align like elongate melanosomes in modern avian feathers. Decay microbes typically populated areas of the feather that were sheltered and relatively secluded from strong flow regimes (therefore, efficacious for attachment an establishment of biofilms, e.g., at platelike barbule surfaces, junction

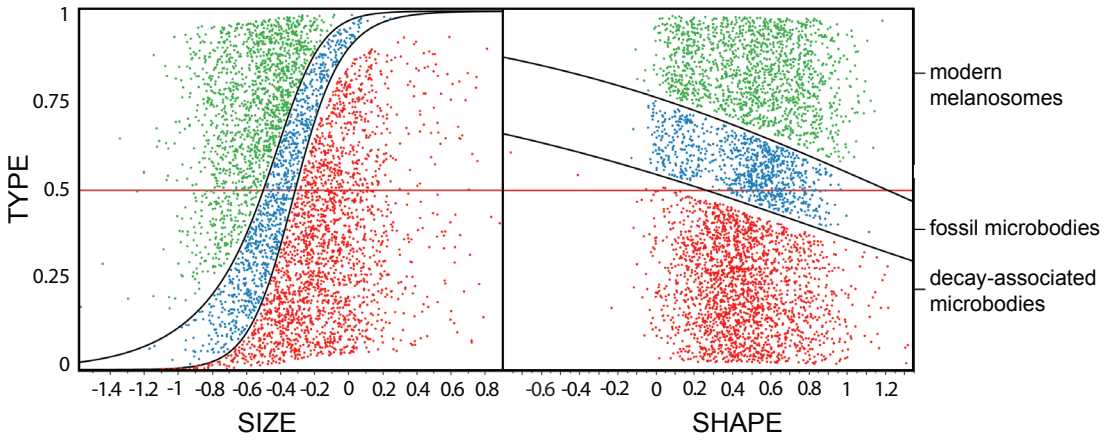

FIG. 2. Logistic fits of "type" against size (χ^2 = 2607.614, p <0.0001) and shape (χ^2 = 56.070, p <0.0001) both statistically significant. Size (R^2 = 0.2730) compared with shape (R^2 = 0.0059) is more important in classification of the collected data into modern melanosomes, fossil microbodies, and decay-associated microbodies.

points between the barbs and rachis, and regions between consecutive barbules). The microbial aggregates were not affected by pigmentation or lack of it, but there are alternate views (Peteya et al., 2017). If the bacterial identity of the microbodies associated with fossil soft tissue is assumed to be true, then the sources of these microbes would have to be an amalgamation of nonsaprotrophic bacteria, obligate and facultative saprotrophic bacteria from the external environment, and endogenous intestinal flora released to surrounding environment by degradation of the integument in the carcass. Studies have illustrated how bacterial communities fluctuate over seasons and temperature regimes (Dickson et al., 2011), and as a result they should encompass a large variety of shapes and sizes, as opposed to more uniform melanosomes and microbodies. Additionally, melanosomes are concentrated in certain tissues and are often structured in a distinct fashion such as alignment of oblong melanosomes along the axes in the feather cortex or barbules (Vinther et al., 2008; Vinther et al., 2010), features also not observed in decay bacteria.

Spherical and subspherical shapes are the most conducive shapes for any membrane-bound structure exposed to osmotic pressure (Jiang et al., 2015), as would be the case for both microbes and subcellular organelles like melanosomes. Moreover, the bacterial samples are a mixed assemblage of geometries. Even if only the rod and spherical shapes are considered, size differences extend over a broad range (a scenario akin to measuring a considerable number of objects of dissimilar sizes), while melanosomes are characteristically more uniform and overlap with fossil microbodies in our PCA plots.

Statistical Analyses of Microbody Geometry

Nonparametric comparisons and PCA of microbody geometry demonstrate that fossil microbodies and microbial cells are significantly dissimilar in shape and size. If the fossil microbodies measured represent melanosomes, differences in geometry between modern melanosomes and fossil microbodies could be due to alteration of melanosome size during diagenesis (Colleary et al., 2015). It has recently been proposed that non-integumentary melanosomes in fossils can be redistributed due to weak lakebed currents and can potentially bias reconstructions of the colors of fossil vertebrates (McNamara et al., 2018). The range of melanosome geometry present in vertebrate tissues has yet to

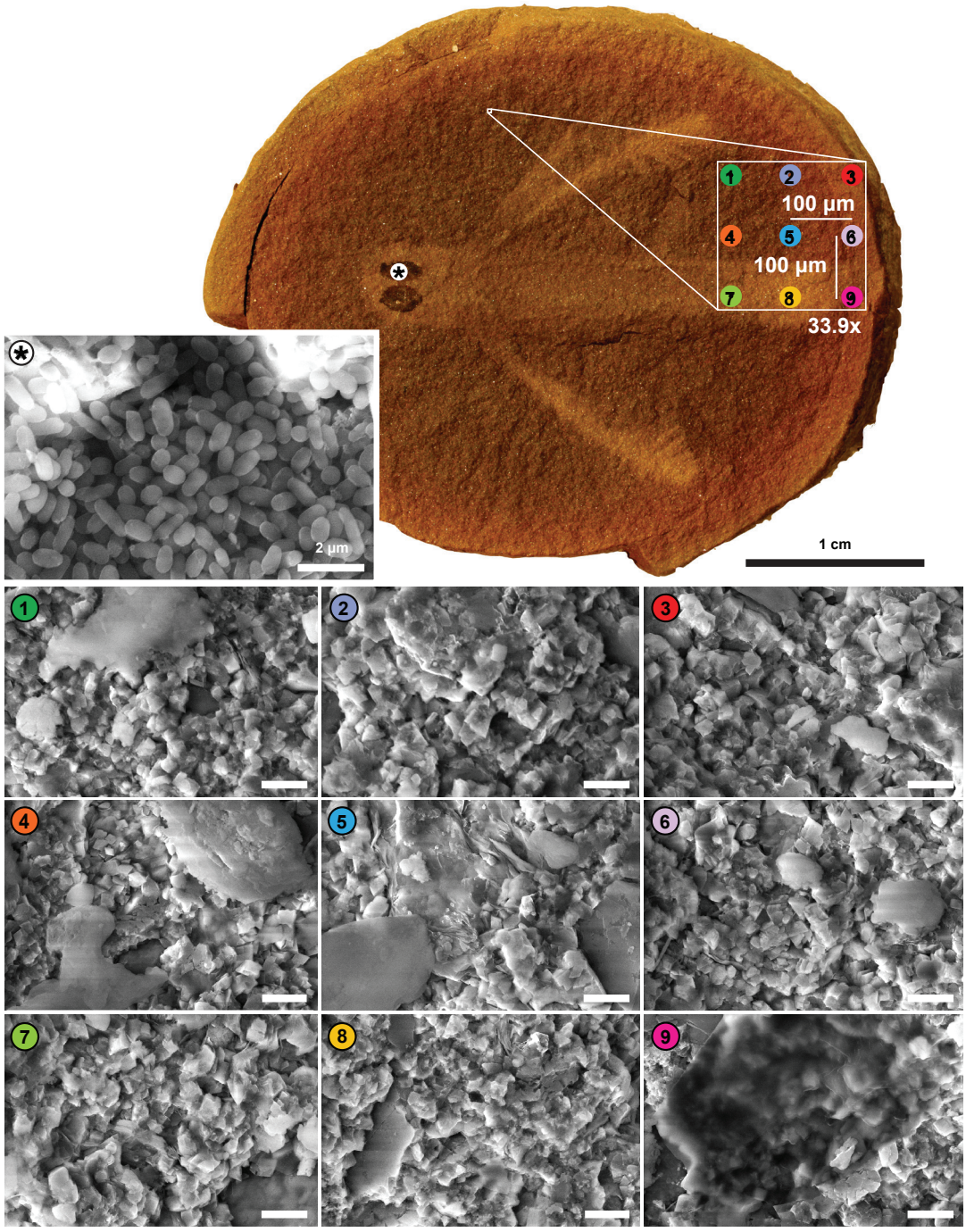

FIG. 3. SEM bedding plane survey for microbodies in the 300 Myr old lungfish *Esconicthys apopyris* (ROM56792), from Mazon Creek, Illinois. The asterisk indicates the region within the outline of the eye, which contains a fabric of microbodies (inset). By contrast, none of the grid points (1–9) show any evidence of such microbodylike structures in the matrix. Scale bars on images = 5 µm.

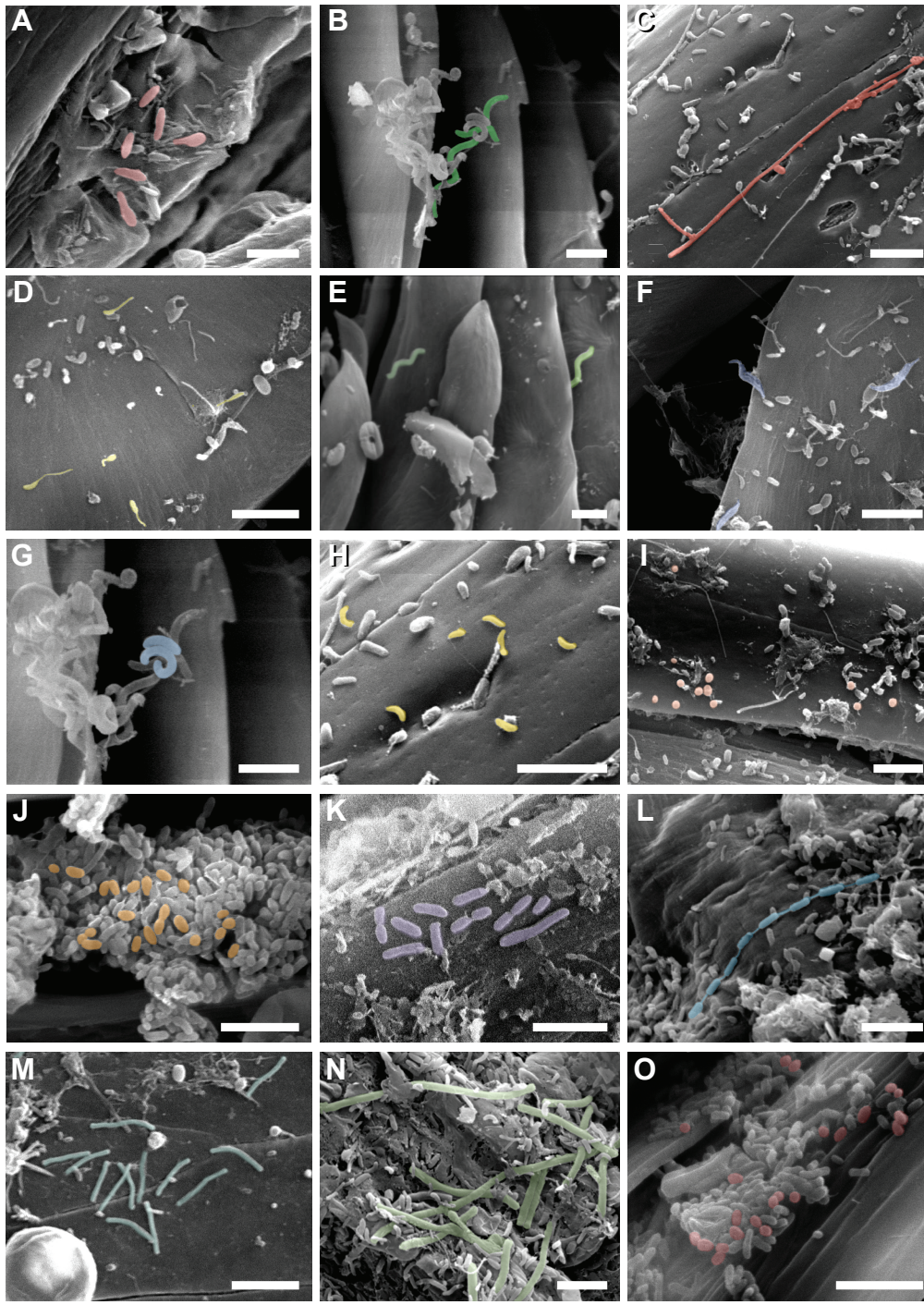

FIG. 4. A wide range of bacterial morphotypes observed in the decay experiments. Bacteria are shown in false colors in the SEM images: **A,** Club rods; **B, E,** spirochaetes; **C, N,** actinomycetes; **D,** flagellated vibrio; **F,** fusiform **G, H,** curved vibrio; **I, J, O,** cocci and coccobacilli; and **K, M,** bacilli; **L,** streptobacilli. Scale bars = 5 μm.

be comprehensively cataloged, although variation in melanosome geometry between tissues and organs is expected to be minimal relative to the geometrical diversity of decay bacteria. Thus, the potential movement of internal melanosomes around the carcass during decay is unlikely to result in consortia of fossil microbodies superficially similar to a community of decay bacteria.

Investigation of Bedding Planes in Exceptionally Preserved Fossils

We surveyed fossil vertebrate material from a range of Lagerstätte localities in which vertebrates are preserved with soft tissues, such as the Cretaceous Jehol Biota from Liaoning, China (Zhang et al., 2010; Chang et al., 2011), the Carboniferous Mazon Creek of Illinois (Clements et al., 2016; Gabbott et al., 2016) and the Eocene Fur and Ølst formations of Denmark (Vinther et al., 2008; Pedersen et al., 2011; Lindgren et al., 2012; Field et al., 2013). These samples represent a multitude of paleoenvironments with varied diagenetic regimes, permitting a robust investigation of the distribution of fossil microbodies. None of the fossil bedding planes investigated showed evidence for microbodies in the surrounding matrix or in tissues that were not originally melanin bearing—fundamentally, fossil microbodies are restricted to specific tissues within the fossil. The lack of microbodies outside of melanin-bearing tissues has also been noted in other studies (Clements et al., 2016; Gabbott et al., 2016). Our findings therefore reject the bacterial hypothesis since decay-associated microbes would be expected to be ubiquitous on the carcass as well as the adjacent sediment, and not restricted to specific tissues. Thus, it can be concluded that it is not common for microbes to fossilize, and particularly not as three-dimensional organic microbodies.

Rare examples of microbes are known from the fossil record, these are mainly restricted to occurrences in which the microbes were entombed alive in rapidly forming cements, such as calcium phosphates (Xiao and Knoll, 1999; Briggs et al., 2005), manganese carbonate (Lozano and Rossi, 2012), amber (Cano and Borucki, 1995; Girard et al., 2009), and chert (Qu et al., 2017). Soft-tissue replacement by authigenic minerals such as calcium phosphate is relatively common in fossil Lagerstätten and generally replicates intestinal tracts (Butterfield, 2002; Vannier et al., 2014), muscle tissue (Briggs et al., 2005; Parry et al., 2015; Wilson et al., 2016; Young et al., 2017), and skin (McNamara et al., 2009; Navalon et al., 2015). Calcium phosphate can preserve tissue and eukaryotic cellular-level fidelity, however, despite the contribution microbes make to the formation of diagenetic and sedimentary calcium phosphate (Briggs, 2003; Crosby and Bailey, 2012), there are few convincing examples of fossilized microbes in this medium (Xiao and Knoll, 1999; Briggs et al., 2005). Examples of microbes that are preserved within manganese carbonates of cave stromatolites are assumed to be due to young ages of the rocks and their lack of diagenesis (Lozano and Rossi, 2012). Silica chert is the most persistent medium for microbial preservation; with bacterial and cyanobacterial fossils documented in rocks from the Archaean (Westall et al., 2001). While cherts commonly preserve microbes, there are limitations to this medium for preservation because precipitation rates vary: increased precipitation through intertidal exposure and the fluctuating conditions will affect the bacterial consortia preserved and intervals with less rapid precipitation often lack microbes altogether (Knoll and Golubic, 1979). Observations of modern hydrothermal systems (Jones et al., 2001, 2004) show that silicification may alter bacterial geometry markedly and may not capture key anatomical features that would allow for confident diagnosis. Thus, even the best taphonomic settings for microbial preservation lead to unreliable and inconsistent preservation of microbes. Most importantly, we know of no microbes fossilized in sedimentary environments that otherwise give way to carbonaceous preservation of cellular organelles like melanosomes.

Melanins beyond the Metazoa: Not All That Is Black, Brown, or Red Is Eumelanin/Pheomelanin

Two prior publications (Lindgren et al., 2015; Schweitzer et al., 2015) have proposed alternative scenarios in which the microbial consortia colonizing decaying carcasses assist in (1) exceptional preservation of carbonaceous films in highly flattened fossils; and (2) the exogenous secretion of extracellular polymeric substances (EPS) and/or melanin by some microbial consortia, in turn, facilitates preservation of these microbial cells, which are being misinterpreted as melanosomes (contra: integumentary melanosomes are the primary cause of preservation of soft tissues in the form of carbonaceous films). However, our review of the literature rules out these alternatives. The term "melanin" has been used rather loosely for several diverse chemical entities. Several attempts to classify these chemicals over the last five decades have occurred (Marks and Seabra, 2001; Prota, 2012), but an all-encompassing definition remains elusive. There are furthermore classes of complex molecules formed from degradation of proteins, sugars, and lipids through Maillard reactions called melanoidins, thought to be involved in kerogen formation (Larter and Douglas, 1980) and are suspected to form inside mollusc shells from their organic shell matrix (Collins et al., 1992). These molecules are, however, compositionally disparate from eu- and pheomelanin. The major enzymes catalysing the synthesis of melanins are tyrosinases, laccases, polyketide synthases, 4-hydroxyphenylacetic acid hydroxylase, and *p*-hydroxyphenylpyruvate oxidase.

The forms of melanin most common to vertebrates—eumelanin and pheomelanin—originate from branches of the catabolic pathway for the amino acids tyrosine and phenylalanine through the action of tyrosinases (Borovansky and Riley, 2011). Forms of melanin more commonly associated with microbial systems are allomelanin and pyomelanin. Allomelanin, also known as 1,8-dihydroxynapthalene (DHN) melanins, is a varied group produced from the precursor Acetyl-CoA via a pathway called pentaketide pathway (Langfelder et al., 2003) via polymerization through action of polyketide synthases, laccases, 4-hydroxyphenylacetic acid hydroxylase (Plonka and Grabacka, 2006), and through oxidation of catecholamines (Wang et al., 1995, 1996). Pyomelanin is produced via part of the tyrosine/phenylalanine catabolism pathway followed by the oxidation and polymerization of homogentisic acid (HGA) through the enzyme *p*-hydroxyphenylpyruvate oxidase (Plonka and Grabacka, 2006).

Several bacterial strains produce allomelanin and pyomelanin. Strains of *Streptomyces* from various environments, marine sources (Vasanthabharathi et al., 2011; Sivaperumal et al., 2014), field soils (Dastager et al., 2006), and limestone quarries (Quadri and Agsar, 2012) are reported to produce melanin/melanoid compounds. These compounds act as alternatives for conventional electron acceptors (Turick et al., 2002), act to prevent UV damage (Plonka and Grabacka, 2006; Gao and Garcia-Pichel, 2011), or enable survival in nutrient-deficient (Chatfield and Cianciotto, 2007; Zheng et al., 2013) and/or hostile environments (Gessler et al., 2014). However, there are instances of microorganisms producing eumelanin/pheomelanin (or slightly similar chemical entities) that function analogously to those of allomelanin and pyomelanin. An *Aeromonas media* strain "WS" isolated from lacustrine settings has been shown to produce elevated levels of melanin (from L-3,4-dihydroxyphenylalanine precursor) (Wan et al., 2007). Other species such as *Marinomonas mediterranea* have been known to possess a two-component melanogenic system, utilizing both tyrosinase (Lopez-Serrano et al., 2002, 2004) and laccase mediated pathways (Solano, 2014), indicating a potential for highly adaptive melanin synthesis.

Strains of *Bacillus*-producing melanin contain active tyrosinases and they become heavily pigmented in the presence of L-tyrosine in the media (Aghajanyan et al., 2005; Drewnowska et al., 2015). *Bacillus subtilis* also synthesizes a brown pigment related to melanin for sporula-

tion, but this process is catalyzed by a laccase-related protein named cot A (Barnett and Hageman, 1983). *Vibrio cholerae* has been reported to produce pyomelanin but switches to eumelanin under stress conditions, like elevated temperatures, hyperosmotic medium, and starvation (Plonka and Grabacka, 2006). One hypertoxic mutant strain of *V. cholerae* HTX-3 has even been described to make pheomelanin (Ivins and Holmes, 1980; 1981). *Streptomyces antibioticus* (a spore-bearing filamentous bacterium) produces eumelanin in which the operon *melC* controls melanin production. The main factor inducing the expression of the *MelC* protein is the amino acid methionine (Chen et al., 1992; Chen et al., 1993). Contrary to the synthesis of animal melanin within well-confined subcellular compartments, bacterial melanin formation usually takes place by autooxidation and subsequent polymerization of the precursors secreted outside the cell (Plonka and Grabacka, 2006).

Fungal melanins are a diverse group of negatively charged, high-molecular-weight hydrophobic pigments (Pombeiro-Sponchiado et al., 2017). Although these pigments are quite common in fungi, their production is limited to certain growth stages on the mycelia, spore formation, or in response to wounding (Bell and Wheeler, 1986). Allomelanin (DHN-melanin) is frequent in ascomycetous fungi and some fungi imperfecti except *Aspergillus niger* and basidiomycetes (Wheeler, 1983). The ascomycete fungi *Cryptococcus neoformans,* a parasite of the central nervous system, produces melanin precursors 3,4-dihydroxyphenylalanine (DOPA) and catecholamines (Wang et al., 1995; Wang et al., 1996) but the chemical nature of the pigments (eumelanin or otherwise) remain contentious (Liu et al., 1999). Basidiomycetes like *Agaricus bisporus* contain a very active tyrosinase enzyme and produce eumelanin from a γ-glutaminyl-4-hydroxybenzene precursor (Solano, 2014), but the process does not take place within the mycelium. Unlike animal melanin, fungal melanin predominantly occurs either as electron-dense granules in extracellular secretions or is deposited within the outermost layer of the chitinous cell wall.

Microbial Melanin Neither Yields Melanosomelike Bodies Nor Is Chemically Identical to Animal Melanins

While the literature is replete with evidence of microorganisms synthesizing allomelanin and pyomelanin, evidence for microbial synthesis of eumelanin and pheomelanin is limited. Melanin synthesis by *V. cholerae* is of particular interest because of the reported switch from pyomelanin to eumelanin production during conditions of stress. The genetic mechanisms for reported production of pheomelanin by the strain *V. cholerae* HTX-3, however, are still pending investigation. The fact that the amino acid methionine is needed to induce the expression of *MelC* protein in *S. antibioticus* is peculiar. Methionine, which forms an integral part of the prokaryotic protein translation machinery, is one of the less abundant amino acids in the prokaryotic metabolome (Pasamontes and Garcia-Vallve, 2006), thus indicating a tightly controlled melanogenic pathway activated only during certain situations (Plonka and Grabacka, 2006).

Fungal melanins perform the same functions as bacterial melanins and are known products that offset stressful environments. Melanization offers defense against UV light and ionizing radiation, and resistance to heat or cold and activity of inorganic antimicrobial compounds, such as silver nitrate (Plonka and Grabacka, 2006). A particularly extreme form of this is observed in certain fungal species, such as *Cladosporium spp*., *Alternaria alternata*, *Aureobasidium pullulans*, and *Hormocornis resinae*, found on the walls of the damaged reactors in Chernobyl, which overproduce melanin to withstand elevated levels of ionizing radiation (Dadachova and Casadevall, 2008; Gessler et al., 2014).

However, none of the aforementioned extremophilic microbes carrying out melanin synthesis have been reported to colonize environs like decaying feathers or carcasses. Additionally, their mode of secretion either extracellularly

or as thin peripheral sheets would not lead to melanosomelike microbodies, which are solidly packed with melanin (apart from some iridescent feathers with hollow melanosomes (Durrer, 1977), which would still have a thicker wall of melanin than those microbes produce. Furthermore, as shown here, these microbes would have different modes of growth and geometry than melanosomes do.

Although it could be argued that the confusion in the differentiation between fossilized microbodies and microbial cells was brought about using biased qualitative-based imaging analysis methods, the current study demonstrates that semiquantitative analysis led to a promising deconvolution of the studied bodies. We acknowledge that body dimensions were manually recorded during SEM image analysis in the hope that future method developments will include automated and standardized image analysis for the interpretation of SEM data from fossils of interest. While semiquantitative analyses of nonfossilized microbodies led to clear distinctions between melanosomes and bacterial bodies, one should also take into account the possibility of artifacts during SEM preparations, and the challenges of properly attributing three-dimensionality to bodies from two-dimensional micrographs. Future differentiation experiments should consider using other methods that allow for proper three-dimensional quantification of microbodies, which would then validate the evidence presented in this study.

Criteria for Fossil Melanin/Melanosome Identification

Since microbes have clear ethological, compositional, and geometrical differences to metazoan melanosomes it is pertinent to evaluate the means of identifying melanin/melanosomes from the fossil record. Melanosomes can be identified by several lines of evidence:

They are localized to certain tissues: In vertebrates, melanosomes are present in the skin and epidermal appendages, such as scales, hair, and feathers (Vinther et al. 2015; Colleary et al., 2015) while some organs, like the eyes, liver, peritoneum, and parts of the nervous system (McNamara et al., 2018; Rossi et al. 2019) have these localized to them. Hence, if the melanosomes form distinct associations that resemble the outline of a feather, liver, or eye, this conforms to a melanosome interpretation.

They may be aligned or layered within said tissues: Melanosomes are oriented in specific directions in different tissues or may be arranged into different layers and this organization has a critical biological function in extant animals (Maia et al., 2012), thus allowing their reliable identification even in fossilized soft tissues. They are likely to occur only in recalcitrant tissues and rarely in exceptionally preserved organs such as the eye. In many soft tissues, decay will result in collapse and potential dispersal of any layers or organization.

Certain taxa may have a limited melanosome geometry: Exemplified in amphibians, the integumentary melanosomes are generally oblate in shape and intermediate between pheomelanosomes and eumelanosomes seen in birds and mammals. Mammals appear to exhibit a more limited diversity of melanosome shape compared to birds (Li et al., 2014), which utilize melanosomes to produce more diverse colors such as structural iridescence and gray, in which the melanosome geometry may play a role in the self-assembly into these conformations (Maia et al., 2012). Very little is known about the true extent of melanosome geometry and arrangements extending across different tissues and taxa; work to address these knowledge gaps in modern animals is currently underway. However, despite the true variety of melanosome geometry being unknown, it is unlikely this variety would exceed that observed in microbes.

Chemical analyses can identify melanin signatures: The most reliable method for identifying melanin in extant samples (Wakamatsu and Ito, 2002) is through permanganate oxidation of eumelanin and hydriodic acid reductive hydrolysis of pheomelanin. This method has been applied

to quantify molecularly intact melanin in Jurassic coleoid ink but is otherwise too destructive for most fossil samples preserving melanin. Another confounding factor is that fossil melanin is diagenetically altered. Other methods provide signatures for melanin such as time of flight–secondary ion mass spectrometry (ToF-SIMS), which provides spectra of molecular ionized fragments that can be visually compared (Lindgren et al., 2012, 2014), or using principal component analyses (Colleary et al., 2015). Colleary et al. (2015) showed that fossil and fresh melanin are distinct in ToF-SIMS, but that artificial maturation experiments yield signatures more similar to fossil spectra. Pyrolysis-GCMS (Py-GCMS) is also valuable for analyzing small amounts of fossil tissue, which yield a suite of distinct markers (Dzierzega-Lecznar et al., 2012; Brown et al., 2017) and the diagenetic alteration of these can also be studied with Py-GCMS (Glass et al., 2012, 2013).

Melanosomes have a distinct geometry: As reviewed herein and presented elsewhere (Vinther et al., 2008, 2010, 2016; Li et al., 2010, 2012), melanosomes present themselves as microstructures with a very distinct geometrical range and have distinct size variation within tissues (Rossi et al., 2019). Their fossilization potential is high, as they have been confidently diagnosed from sample fossil tissues as old as Carboniferous (300 Myr) (Clements et al., 2016; Gabbott et al., 2016) and can leave impressions in the matrix cement when secondarily oxidized.

In total, several lines of evidence are available to detect melanin, and only a subset of these is necessary to diagnose its presence. While a single piece of evidence is persuasive by itself, separate lines of evidence (congruence) make the judgment stronger and this is generally advocated. It has been argued that chemical analyses are warranted in every instance because microbes and melanosomes are indistinguishable (Lindgren et al., 2012, 2014, 2015). Given the evidence presented here, this perspective cannot be justified based on those assumptions. To simply diagnose the preservation of melanin or melanosomes, identifying their distinct microbodies and observing their presence in tissues that are known to be melanin bearing is adequate as separate lines of evidence on which to make a judgment. This allows for diagnosis of melanosomes even when they are not preserved organically, but only as impressions. However, sometimes melanosome geometries are lost, and the melanin has merged into a solid mass (Carney et al., 2012). In these instances, chemical analyses may be helpful in providing a complementary line of evidence in addition to patterns of distribution (Brown et al., 2017). Likewise, if melanosomes are found outside a tissue that is assumed to be melanin bearing, then chemical analyses may be advisable (Vinther et al., 2016).

There is still much to be learnt about the relative stability and survival of melanins through diagenesis and geological time; a question also remains as to whether eumelanin and pheomelanin have different survival potentials. Chemical surveys should aim to synthesize evidence in larger frameworks rather than targeting single specimens for the sake of diagnosing it as melanin bearing or not (Gren et al., 2017).

CONCLUSIONS

The results of this study demonstrate that the interpretation of microbodies in fossil vertebrate tissues as microbes (Moyer et al., 2014; Lindgren et al., 2015; Schweitzer et al., 2015) cannot be justified and that they conform to melanosomes in terms of shape and size. During decay experiments, microbes are not localized to melanin-bearing tissues, nor do they exhibit the ordered arrangement common to extant melanosomes. Conversely, in fossil material, the microbodies are restricted to tissues known to be melanosome rich in vivo. The microbodies are not present in the adjacent matrix or continuously across boundaries of melanized and unmelanized tissues—contradicting a bacterial diagnosis. The geometry (Ivins and Holmes, 1980; 1981; Chen et al., 1992, 1993), mode of secretion (Plonka and Grabacka, 2006; Solano, 2014), and chemical composition (Wang et al., 1995; Wang et al.,

1996; Plonka and Grabacka, 2006) of melanin-synthesizing microbes would also negate any conflation with melanosomes.

Based on our results, we reject all four of our original hypotheses: (1) melanosomes and microbial cells are geometrically indistinguishable; (2) microbes localize and align themselves in orientations akin to extant melanosomes; (3) microbes fossilize easily and are thus ubiquitous throughout fossils; and (4) microbes are sources of melanin and there is a likelihood of extraneous preservation in fossils. The rejection of hypotheses 1–4 strongly upholds the interpretation of fossil microbodies as melanosomes. Additionally, as multiple lines of evidence support melanosome identification, we suggest that only a subset of these evidence sources are necessary for the interpretation of fossil melanin and its use in inferring tissue identity, structure, evolution, and color.

ACKNOWLEDGMENTS

We would like to thank Bel Deering of the RSPCA West Hatch Animal Centre (Taunton, U.K.) for providing us with carcasses of deceased birds for our decay studies. We thank the Royal Ontario Museum, Toronto, Canada. the Field Museum of Natural History, Chicago, the Lauer Foundation PSE and the Burpee Museum, Rockford, IL, for their loans of Mazon Creek fossil material to T.C. We would also like to thank Klara Norden (Department of Ecology and Evolutionary Biology, Princeton University, NJ.), Jaeike W. Faber (Department of Medical Biology, Amsterdam Cardiovascular Sciences, Amsterdam UMC, University of Amsterdam, Amsterdam, The Netherlands) and Frane Babarović (Department of Animal and Plant Sciences, University of Sheffield, Sheffield, U.K.) for modern melanosome samples, Fiann Smithwick (School of Earth Sciences, University of Bristol, Bristol, U.K.) for fossil microbody samples from the Grube Messel Lagerstätte, and David Marshall (School of Earth Sciences, University of Bristol) for assistance regarding the collection of sediment inocula from the Severn Estuary. Further thanks to Michael Benton (School of Earth Sciences, University of Bristol), Stuart Kearns (School of Earth Sciences, University of Bristol) and Zhang Fucheng (Institute of Geology and Paleontology, Linyi University, Linyi, China) for access to the fossil feather specimen IVPP V15388B; and to John Bacon-Shone (Faculty of Social Sciences, the University of Hong Kong, Hong Kong SAR, China) for helping A.R. with the statistical analysis. Evan Saitta (Field Museum, Chicago, IL), Benjamin Moon and Tom Stubbs (School of Earth Sciences, University of Bristol) are thanked for discussions and suggestions. This study was supported by funds from the Bob Savage Memorial Fund (School of Earth Sciences, University of Bristol) to A.R., Hong Kong Ph.D. Fellowship 2017-18 (PF16-09281) to A.R., and a Royal Society Research Grant RG15042 to J.V. Conference presentations made by A.R. helped to improve the study and were supported by the Palaeontological Association Postgraduate Travel Fund (Grants-in-Aid scheme) and a University of Bristol Alumni Foundation Travel Grant.

REFERENCES

Aghajanyan, A.E., et al. 2005. Isolation, purification and physicochemical characterization of water-soluble *Bacillus thuringiensis* melanin. Pigment Cell & Melanoma Research 18: 130–135.

Barnett, T.A., and J.H. Hageman. 1983. Characterization of a brown pigment from *Bacillus subtilis* cultures. Canadian Journal of Microbiology 29: 309–315.

Bell, A.A., and M.H. Wheeler. 1986. Biosynthesis and functions of fungal melanins. Annual Review of Phytopathology 24: 411–451.

Bonde, N.C. 1997. An Upper Paleocene *Antigonia*-like fish from Denmark: and its relations to other advanced teleosteans. Bulletin of the Geological Society of Denmark 9710-0100.

Borovansky, J., and P.A. Riley. 2011. Melanins and melanosomes: biosynthesis, structure, physiological and pathological functions. Weinheim: Wiley-VCH.

Briggs, D.E.G. 2003. The role of decay and mineralization in the preservation of soft-bodied fossils. Annual Review of Earth and Planetary Sciences 31: 275–301.

Briggs, D.E.G., and P.R. Crowther. 2008. Palaeobiology II. Oxford: John Wiley & Sons.

Briggs, D.E.G., R.A. Moore, J.W. Shultz, and G. Schweigert. 2005. Mineralization of soft-part anatomy and invading microbes in the horseshoe crab *Mesolimulus* from the Upper Jurassic Lagerstatte of Nusplingen, Germany. Proceedings of the Royal Society B, Biological Sciences 272: 627–632.

Brown, C.M., et al. 2017. An exceptionally preserved three-dimensional armored dinosaur reveals insights into coloration and Cretaceous predator-prey dynamics. Current Biology 27: 2514–2521.

Burley, N., G. Krantzberg, and P. Radman. 1982. Influence of colour-banding on the conspecific preferences of zebra finches. Animal Behaviour 30: 444–455.

Butcher, G.S., and S. Rohwer. 1989. The evolution of conspicuous and distinctive coloration for communication in birds. *In* D.M. Power (editor), Current Ornithology, vol. 6: 51–108. Boston: Springer.

Butterfield, N.J. 2002. *Leanchoilia* guts and the interpretation of three-dimensional structures in Burgess Shale-type fossils. Paleobiology 28: 155–171.

Cano, R., and M. Borucki. 1995. Revival and identification of bacterial spores in 25- to 40-million-year-old Dominican amber. Science 268: 1060–1064.

Carney, R.M., J. Vinther, M.D. Shawkey, L. D'Alba, and J. Ackermann. 2012. New evidence on the colour and nature of the isolated *Archaeopteryx* feather. Nature Communications 3: 637.

Chang, M.M., P.J. Chen, Y. Wang, and Y.Q. Wang. 2011. The Jehol fossils: the emergence of feathered dinosaurs, beaked birds and flowering plants, London: Academic Press.

Chatfield, C.H., and N.P. Cianciotto. 2007. The secreted pyomelanin pigment of *Legionella pneumophila* confers ferric reductase activity. Infection and Immunity 75: 4062–4070.

Chen, L.Y., W.M. Leu, K.T. Wang, and Y.H. Lee. 1992. Copper transfer and activation of the *Streptomyces* apotyrosinase are mediated through a complex formation between apotyrosinase and its *trans*-activator MelC1. Journal of Biological Chemistry 267: 20100–20107.

Chen, L.Y., M.Y. Chen, W.M. Leu, T.Y. Tsai, and Y.H. Lee. 1993. Mutational study of *Streptomyces* tyrosinase *trans*-activator MelC1. MelC1 is likely a chaperone for apotyrosinase. Journal of Biological Chemistry 268: 18710–18716.

Clarke, J.A., et al. 2010. Fossil evidence for evolution of the shape and color of penguin feathers. Science 330: 954–957.

Clements, T., et al. 2016. The eyes of *Tullimonstrum* reveal a vertebrate affinity. Nature 532: 500–503.

Colleary, C., et al. 2015. Chemical, experimental, and morphological evidence for diagenetically altered melanin in exceptionally preserved fossils. Proceedings of the National Academy of Sciences of the United States of America 112: 12592–12597.

Collins, M.J., P. Westbroek, G. Muyzer, and J.W. de Leeuw. 1992. Experimental evidence for condensation reactions between sugars and proteins in carbonate skeletons. Geochimica et Cosmochimica Acta 56: 1539–1544.

Crosby, C.H., and J.V. Bailey. 2012. The role of microbes in the formation of modern and ancient phosphatic mineral deposits. Frontiers in Microbiology 3: 241.

Cuthill, I.C., et al. 2017. The biology of color. Science 357: eaan0221.

Dadachova, E., and A. Casadevall. 2008. Ionizing radiation: how fungi cope, adapt, and exploit with the help of melanin. Current Opinion in Microbiology 11: 525–531.

Dastager, S.G., et al. 2006. Seperation, identification and analysis of pigment (melanin) production in *Streptomyces*. African Journal of Biotechnology 5: 1131–1134.

Dickson, G.C., R.T. Poulter, E.W. Maas, P.K. Probert, and J.A. Kieser. 2011. Marine bacterial succession as a potential indicator of postmortem submersion interval. Forensic Science International 209: 1–10.

Drewnowska, J.M., M. Zambrzycka, B. Kalska-Szostko, K. Fiedoruk, and I. Swiecicka. 2015. Melanin-like pigment synthesis by soil *Bacillus weihenstephanensis* isolates from Northeastern Poland. PLoS One 10: e0125428.

Durrer, H. 1977 Schillerfarben der vogelfeder als evolutionsproblem. Denkschriften der Schweizerischen Naturforschenden Gesellschaft 91: 1–127.

Dzierzega-Lecznar, A., S. Kurkiewicz, and K. Stepien. 2012. Detection and quantitation of a pheomelanin component in melanin pigments using pyrolysis-gas chromatography/tandem mass spectrometry system with multiple reaction monitoring mode. Journal of Mass Spectrometry 47: 242–245.

Field, D.J., et al. 2013. Melanin concentration gradients in modern and fossil feathers. PLoS One 8: e59451.

Gabbott, S.E., et al. 2016. Pigmented anatomy in Carboniferous cyclostomes and the evolution of the vertebrate eye. Proceedings of the Royal Society B, Biological Sciences 283: rspb.2016.1151.

Gao, Q., and F. Garcia-Pichel. 2011. Microbial ultraviolet sunscreens. Nature Reviews Microbiology 9: 791–802.

Gessler, N.N., A.S. Egorova, and T.A. Belozerskaia. 2014. Melanin pigments of fungi under extreme environmental conditions Prikladnaia Biokhimiia i Mikrobiologiia 50: 125–134.

Girard, V., et al. 2009. Taphonomy and palaeoecology of mid-Cretaceous amber-preserved microorganisms from southwestern France. Geodiversitas 31: 153–162.

Glass, K., et al. 2012. Direct chemical evidence for eumelanin pigment from the Jurassic period. Proceedings of the National Academy of Sciences of the United States of America 109: 10218–10223.

Glass, K., et al. 2013. Impact of diagenesis and maturation on the survival of eumelanin in the fossil record. Organic Geochemistry 64: 29–37.

Gren, J.A., et al. 2017. Molecular and microstructural inventory of an isolated fossil bird feather from the Eocene Fur Formation of Denmark. Palaeontology 60: 73–90.

Hill, G.E., and K.J. McGraw. 2006a. Bird coloration, vol. 2: function and evolution. Cambridge: Harvard University Press.

Hill, G.E., and K.J. McGraw. 2006b. Bird coloration, vol. 1: mechanisms and measurements. Cambridge: Harvard University Press.

Hu, D.Y., et al. 2018. A bony-crested Jurassic dinosaur with evidence of iridescent plumage highlights complexity in early paravian evolution. Nature Communications 9: 217.

Ichida, J.M., et al. 2001. Bacterial inoculum enhances keratin degradation and biofilm formation in poultry compost. Journal of Microbiological Methods 47: 199–208.

Ito, S. & Wakamatsu, K. (2003). Quantitative analysis of eumelanin and pheomelanin in humans, mice, and other animals: a comparative review. Pigment Cell Research 16: 523–531.

Ivins, B.E., and R.K. Holmes. 1980. Isolation and characterization of melanin-producing (mel) mutants of *Vibrio cholerae*. Infection and Immunity 27: 721–729.

Ivins, B.E., and R.K. Holmes. 1981. Factors affecting phaeomelanin production by a melanin-producing (mel) mutant of *Vibrio cholerae*. Infection and Immunity 34: 895–899.

Jiang, C., P.D. Caccamo, and Y.V. Brun. 2015. Mechanisms of bacterial morphogenesis: evolutionary cell biology approaches provide new insights. Bioessays 37: 413–425.

Jones, B., R.W. Renaut, and M.R. Rosen. 2001. Taphonomy of silicified filamentous microbes in modern geothermal sinters—implications for identification. Palaios 16: 580–592.

Jones, B., K.O. Konhauser, R.W. Renaut, and R.S. Wheeler. 2004. Microbial silicification in Iodine Pool, Waimangu geothermal area, North Island, New Zealand: implications for recognition and identification of ancient silicified microbes. Journal of the Geological Society 161: 983–993.

Knoll, A.H., and S. Golubic. 1979. Anatomy and taphonomy of a Precambrian algal stromatolite. Precambrian Research 10: 115–151.

Kowalewski, M. 1999. Actuopaleontology: the strength of its limitations. Acta Palaeontologica Polonica 44: 452–454.

Langfelder, K., M. Streibel, B. Jahn, G. Haase, and A.A. Brakhage. 2003. Biosynthesis of fungal melanins and their importance for human pathogenic fungi. Fungal Genetics and Biology 38: 143–158.

Larter, S.R., and A.G. Douglas. 1980. Melanoidins—kerogen precursors and geochemical lipid sinks—a study using pyrolysis-gas chromatography (Pgc). Geochimica et Cosmochimica Acta 44: 2087–2095.

Lehmann, E.L. 2006. Nonparametrics: statistical methods based on ranks. New York: Springer.

Li, Q., et al. 2010. Plumage color patterns of an extinct dinosaur. Science 327: 1369–1372.

Li, Q., et al. 2012. Reconstruction of *Microraptor* and the evolution of iridescent plumage. Science 335: 1215–1219.

Li, Q., et al. 2014. Melanosome evolution indicates a key physiological shift within feathered dinosaurs. Nature 507: 350–353.

Lindgren, J., et al. 2012. Molecular preservation of the pigment melanin in fossil melanosomes. Nature Communications 3: 824.

Lindgren, J., et al. 2014. Skin pigmentation provides evidence of convergent melanism in extinct marine reptiles. Nature 506: 484–488.

Lindgren, J., et al. 2015. Interpreting melanin-based coloration through deep time: a critical review. Proceedings of the Royal Society B, Biological Sciences 282: rspb.2015.0614.

Liu, L.D., K. Wakamatsu, S. Ito, and P.R. Williamson. 1999. Catecholamine oxidative products, but not melanin, are produced by *Cryptococcus neoformans* during neuropathogenesis in mice. Infection and Immunity 67: 108–112.

Lopez-Serrano, D., A. Sanchez-Amat, and F. Solano. 2002. Cloning and molecular characterization of a SDS-activated tyrosinase from *Marinomonas mediterranea*. Pigment Cell and Melanoma Research 15: 104–111.

Lopez-Serrano, D., F. Solano, and A. Sanchez-Amat. 2004. Identification of an operon involved in tyrosinase activity and melanin synthesis in *Marinomonas mediterranea*. Gene 342: 179–187.

Lozano, R.P., and C. Rossi. 2012. Exceptional preservation of Mn-oxidizing microbes in cave stromatolites (El Soplao, Spain). Sedimentary Geology 255: 42–55.

Maia, R., R.H. Macedo, and M.D. Shawkey. 2012. Nanostructural self-assembly of iridescent feather barbules through depletion attraction of melanosomes during keratinization. Journal of the Royal Society Interface 9: 734–743.

Manning, P.L., et al. 2019. Pheomelanin pigment remnants mapped in fossils of an extinct mammal. Nature Communications 10: 2250.

Marks, M.S., and M.C. Seabra. 2001. The melanosome: membrane dynamics in black and white. Nature Reviews Molecular Cell Biology 2: 738–748.

McNamara, M.E., et al. 2009. Soft-tissue preservation in Miocene frogs from Libros, Spain: insights into the genesis of decay microenvironments. Palaios 24: 104–117.

McNamara, M.E., et al. 2016. Fossilization of melanosomes via sulfurization. Palaeontology 59: 337–350.

McNamara, M.E., et al. 2018. Non-integumentary melanosomes can bias reconstructions of the colours of fossil vertebrates. Nature Communications 9: 2878.

Moyer, A.E., et al. 2014. Melanosomes or microbes: testing an alternative hypothesis for the origin of microbodies in fossil feathers. Scientific Reports 4: 4233.

Navalón, G., J. Marugan-Lobon, L.M. Chiappe, J. Luis Sanz, and A.D. Buscalioni. 2015. Soft-tissue and dermal arrangement in the wing of an Early Cretaceous bird: implications for the evolution of avian flight. Scientific Reports 5: 14864.

Neuhäuser, M., and F. Bretz. 2001. Nonparametric all-pairs multiple comparisons. Biometrical Journal: Journal of Mathematical Methods in Biosciences 43: 571–580.

Pan, Y., et al. 2016. Molecular evidence of keratin and melanosomes in feathers of the Early Cretaceous bird *Eoconfuciusornis*. Proceedings of the National Academy of Sciences of the United States of America 113: E7900–E7907.

Parry, L.A., P. Wilson, D. Sykes, G.D. Edgecombe, and J. Vinther. 2015. A new fireworm (Amphinomidae) from the Cretaceous of Lebanon identified from three-dimensionally preserved myoanatomy. BMC Evolutionary Biology 15: 256.

Pasamontes, A., and S. Garcia-Vallve. 2006. Use of a multi-way method to analyze the amino acid composition of a conserved group of orthologous proteins in prokaryotes. BMC Bioinformatics 7: 257.

Pedersen, G.K., et al. 2011. Moleområdets geologi – sedimenter, fossiler, askelagog glacialtektonik. Geologisk Tidsskrift: 41–135.

Peteya, J.A., J.A. Clarke, Q.G. Li, K.Q. Gao, and M.D. Shawkey. 2017. The plumage and colouration of an enantiornithine bird from the Early Cretaceous of China. Palaeontology 60: 55–71.

Plonka, P.M., and M. Grabacka. 2006. Melanin synthesis in microorganisms—biotechnological and medical aspects. Acta Biochimica Polonica 53: 429–443.

Pombeiro-Sponchiado, S.R., G.S. Sousa, J.C.R. Andrade, H.F. Lisboa, and R.C.R. Gonçalves. 2017. Production of melanin pigment by fungi and its biotechnological applications. *In* M. Blumenberg (editor), Melanin: 47–75. London: InTech.

Prota, G. 2012. Melanins and melanogenesis. San Diego: Academic Press.

Prum, R.O. 1999. The anatomy and physics of avian structural colours. *In* N. Adams and R. Slotow (editors), Proceedings of the 22nd International Ornithological Congress 16–22 August 1998, Durban, "Making rain for African ornithology": 1633–1653. Johannesburg: BirdLife South Africa.

Qu, Y.G., et al. 2017. Carbonaceous biosignatures of diverse chemotrophic microbial communities from chert nodules of the Ediacaran Doushantuo Formation. Precambrian Research 290: 184–196.

Quadri, S.R., and D. Agsar. 2012. Detection of melanin producing thermo-alkaliphilic *Streptomyces* from limestone quarries of the Deccan traps. World Journal of Science and Technology 2: 8–12.

Raposo, G., D. Tenza, D.M. Murphy, J.F. Berson, and M.S. Marks. 2001. Distinct protein sorting and localization to premelanosomes, melanosomes, and lysosomes in pigmented melanocytic cells. Journal of Cell Biology 152: 809–824.

Rossi, V., M.E. McNamara, S.M. Webb, S. Ito, and K. Wakamatsu. 2019. Tissue-specific geometry and chemistry of modern and fossilized melanosomes reveal internal anatomy of extinct vertebrates. Proceedings of the National Academy of Sciences of the United States of America: 201820285.

Roy, A., M. Pittman, E.T. Saitta, T.G. Kaye, and X. Xu. 2020. Recent advances in amniote palaeocolour reconstruction and a framework for future research. Biological Reviews 95: 22–50.

Sansom, R.S. 2014. Experimental decay of soft tissues. Paleontological Society Papers 20: 259–274.

Schneider, C.A., W.S. Rasband, and K.W. Eliceiri. 2012. NIH Image to ImageJ: 25 years of image analysis. Nature Methods 9: 671–675.

Schweitzer, M.H., J. Lindgren, and A.E. Moyer. 2015. Melanosomes and ancient coloration re-examined: a response to Vinther 2015. Bioessays 37: 1174–1183.

Sivaperumal, P., K. Kamala, R. Rajaram, and S.S. Mishra. 2014. Melanin from marine *Streptomyces* sp. (MVCS13) with potential effect against ornamental fish pathogens of *Carassius auratus* (Linnaeus, 1758). Biocatalysis and Agricultural Biotechnology 3: 134–141.

Smithwick, F.M., R. Nicholls, I.C. Cuthill, and J. Vinther. 2017. Countershading and stripes in the theropod dinosaur *Sinosauropteryx* reveal heterogeneous habitats in the Early Cretaceous Jehol Biota. Current Biology 27: 3337–3343.

Solano, F. 2014. Melanins: skin pigments and much more—types, structural models, biological functions, and formation routes. New Journal of Science 2014: 1–28.

Suvarna, K., C. Layton, and J. Bancroft. 2019. Bancroft's theory and practice of histological techniques. Amsterdam: Elsevier.

Tanaka, G., et al. 2014. Mineralized rods and cones suggest colour vision in a 300 Myr-old fossil fish. Nature Communications 5: 5920.

Thibaudeau, G. & Altig, R. (2012). Coloration of anuran tadpoles (Amphibia): development, dynamics, function, and hypotheses. ISRN Zoology 2012: 1–16.

Toporski, J.K.W., et al. 2002. Morphologic and spectral investigation of exceptionally well-preserved bacterial biofilms from the Oligocene Enspel formation, Germany. Geochimica et Cosmochimica Acta 66: 1773–1791.

Turick, C.E., L.S. Tisa, and F. Caccavo Jr. 2002. Melanin production and use as a soluble electron shuttle for Fe(III) oxide reduction and as a terminal electron acceptor by *Shewanella algae* BrY. Applied and Environmental Microbiology 68: 2436–2444.

Valentine, J.W. 1989. How good was the fossil record? Clues from the Californian Pleistocene. Paleobiology 15: 83–94.

Vannier, J., J. Liu, R. Lerosey-Aubril, J. Vinther, and A.C. Daley. 2014. Sophisticated digestive systems in early arthropods. Nature Communications 5: 3641.

Vasanthabharathi, V., R. Lakshminarayanan, and S. Jayalakshmi. 2011. Melanin production from marine *Streptomyces*. African Journal of Biotechnology 10: 11224–11234.

Vinther, J. 2015. A guide to the field of palaeo colour—melanin and other pigments can fossilise: reconstructing colour patterns from ancient organisms can give new insights to ecology and behaviour. Bioessays 37: 643–656.

Vinther, J. 2016. Fossil melanosomes or bacteria? A wealth of findings favours melanosomes: melanin fossilises relatively readily, bacteria rarely, hence the need for clarification in the debate over the identity of microbodies in fossil animal specimens. Bioessays 38: 220–225.

Vinther, J. 2020. Reconstructing vertebrate paleocolor. Annual Reviews of Earth and Planetary Sciences 48: 14.1–14.31.

Vinther, J., D.E.G. Briggs, R.O. Prum, and V. Saranathan. 2008. The colour of fossil feathers. Biology Letters 4: 522–525.

Vinther, J., D.E.G. Briggs, J. Clarke, G. Mayr, and R.O. Prum. 2010. Structural coloration in a fossil feather. Biology Letters 6: 128–131.

Vinther, J., et al. 2016. 3D camouflage in an ornithischian dinosaur. Current Biology 26: P2456–2462.

Wakamatsu, K., and S. Ito. 2002. Advanced chemical methods in melanin determination. Pigment Cell and Melanoma Research 15: 174–183.

Wan, X., et al. 2007. Isolation of a novel strain of *Aeromonas media* producing high levels of DOPA-melanin and assessment of the photoprotective role of the melanin in bioinsecticide applications. Journal of Applied Microbiology 103: 2533–2541.

Wang, Y.L., P. Aisen, and A. Casadevall. 1995. *Cryptococcus neoformans* melanin and virulence: mechanism of action. Infection and Immunity 63: 3131–3136.

Wang, Y.L., P. Aisen, and A. Casadevall. 1996. Melanin, melanin "ghosts," and melanin composition in *Cryptococcus neoformans*. Infection and Immunity 64: 2420–2424.

Westall, F., et al. 2001. Early Archean fossil bacteria and biofilms in hydrothermally-influenced sediments from the Barberton greenstone belt, South Africa. Precambrian Research 106: 93–116.

Wheeler, M.H. 1983. Comparisons of fungal melanin biosynthesis in Ascomycetous, imperfect and Basidiomycetous fungi. Transactions of the British Mycological Society 81: 29–36.

Wilson, P., L.A. Parry, J. Vinther, G.D. Edgecombe, and S. Gabbott. 2016. Unveiling biases in soft-tissue

phosphatization: extensive preservation of musculature in the Cretaceous (Cenomanian) polychaeteRollinschaeta myoplena(Annelida: Amphinomidae). Palaeontology 59: 463–479.

Wuttke, M. 1983. Weichteil-Erhaltung'durch lithifizierte Mikroorganismen bei mittel-eozänen Vertebraten aus den Ölschiefern der 'Grube Messel'bei Darmstadt. Senckenbergiana Lethaea 64: 509–527.

Xiao, S., and A.H. Knoll. 1999. Fossil preservation in the Neoproterozoic Doushantuo phosphorite Lagerstatte, South China. Lethaia 32: 219–240.

Xu, X., et al. 2015. A bizarre Jurassic maniraptoran theropod with preserved evidence of membranous wings. Nature 521: 70–73.

Yap, B.W., and C.H. Sim. 2011. Comparisons of various types of normality tests. Journal of Statistical Computation and Simulation 81: 2141–2155.

Young, F.J., J. Vinther, and X.G. Zhang. 2017. Onychophoran-like myoanatomy of the Cambrian gilled lobopodian *Pambdelurion whittingtoni*. Palaeontology 60: 27–54.

Zhang, F.C., et al. 2010. Fossilized melanosomes and the colour of Cretaceous dinosaurs and birds. Nature 463: 1075–1078.

Zheng, H., C.H. Chatfield, M.R. Liles, and N.P. Cianciotto. 2013. Secreted pyomelanin of *Legionella pneumophila* promotes bacterial iron uptake and growth under iron-limiting conditions. Infection and Immunity 81: 4182–4191.

Zheng, X.T., et al. 2017. Exceptional preservation of soft tissue in a new specimen of *Eoconfuciusornis* and its biological implications. National Science Review 4: 441–452.

Zuschin, M., and C. Ebner. 2015. Actuopaleontological characterization and molluscan biodiversity of a protected tidal flat and shallow subtidal at the northern Red Sea. Facies 61: 5.